PNAS RESEARCH ARTICLE | APPLIED BIOLOGICAL SCIENCES

Long noncoding RNA MALAT1 is dynamically regulated in leader cells during collective cancer invasion

Ninghao Zhu[a], Mona Ahmed[a], Yanlin Li[b], Joseph C. Liao[c], and Pak Kin Wong[a,d,e,1]

Edited by David Weitz, Harvard University, Cambridge, MA; received April 3, 2023; accepted May 13, 2023

Cancer cells collectively invade using a leader–follower organization, but the regulation of leader cells during this dynamic process is poorly understood. Using a dual double-stranded locked nucleic acid (LNA) nanobiosensor that tracks long noncoding RNA (lncRNA) dynamics in live single cells, we monitored the spatiotemporal distribution of lncRNA during collective cancer invasion. We show that the lncRNA MALAT1 (metastasis-associated lung adenocarcinoma transcript 1) is dynamically regulated in the invading fronts of cancer cells and patient-derived spheroids. MALAT1 transcripts exhibit distinct abundance, diffusivity, and distribution between leader and follower cells. MALAT1 expression increases when a cancer cell becomes a leader and decreases when the collective migration process stops. Transient knockdown of MALAT1 prevents the formation of leader cells and abolishes the invasion of cancer cells. Taken together, our single-cell analysis suggests that MALAT1 is dynamically regulated in leader cells during collective cancer invasion.

metastasis | lncRNA | bladder cancer | single cell analysis | biosensor

Collective invasion is increasingly recognized as a predominant mechanism in cancer metastasis (1). In particular, specialized cancer cells at invading fronts of tumors, termed as "leader cells", generate invasion paths, coordinate follower cells, and enhance survival in the metastatic cascade by engaging various mechanical, genetic, and metabolomic programs (2). Genetic and epigenetic factors, stromal cells, and matrix properties have all been shown to promote the formation of leader cells and modulate their functions (3–6). Leader cells can switch positions with follower cells during invasion (7), and the ablation of leader cells initiates new leader cells (8), underscoring the time-dependent and competitive nature of leader cell regulation. Nevertheless, how leader cells are dynamically regulated during collective cancer invasion remains largely unknown.

Long noncoding RNAs (lncRNAs), which are nonprotein-coding RNA transcripts over 200 nucleotides, have been implicated in the progression and metastasis of cancer (9, 10). Despite lacking the protein-coding potential, lncRNAs can control gene expression via various mechanisms, such as regulating chromatin modifying enzymes in epigenetic regulation, perturbing alternative splicing in posttranscriptional regulation, and modulating cytoplasmic RNA or protein in posttranslational regulation (11–13). Several lncRNAs, such as metastasis-associated lung adenocarcinoma transcript 1 (MALAT1) and urothelial cancer-associated 1 (UCA1), are reported to modulate cancer progression and metastasis (9, 14–16). For instance, MALAT1 promotes metastasis of lung, bladder, and other cancers by regulating metastasis-associated genes and changing splicing patterns (17–20). Paradoxically, MALAT1 is also reported to suppress metastasis in colon and breast cancers by inactivating prometastatic transcription factors and modulating epithelial-mesenchymal transition (EMT) (21–24). These conflicting reports highlight the multifunctionalities of lncRNA in cancer and the challenges of studying the function of lncRNAs, calling for technologies that can better resolve the actions of lncRNA.

This study develops a nanobiosensor for probing lncRNA dynamics in live cancer cells during collective cancer invasion. Since leader cells represent only a small subset of cancer cells, live single-cell biosensors with a high spatiotemporal resolution are required for investigating the function of lncRNA (25–28). However, existing techniques, such as RNA sequencing and RNA fluorescence in situ hybridization (FISH) that lyse or fix the samples (25, 29, 30), fail to reveal the spatial and temporal dynamics of RNAs in cancer cells during collective cancer invasion. Here, we demonstrate a dual double-stranded lock nucleic acid (dsLNA) nanobiosensor based on fluorescence resonance energy transfer (FRET) for dynamic lncRNA analysis in live single cells in two-dimensional (2D) and three-dimensional (3D) invasion models. We characterize the role of MALAT1 in leader cell formation and cancer invasion using the nanobiosensor. Single-molecule tracking determined the abundance, distribution, and dynamics of lncRNA transcripts in leader and follower cells. The expression of MALAT1 was monitored in 3D spheroids derived

Significance

The prevalence of collective cancer invasion as a mechanism of cancer metastasis is widely reported, but the regulatory mechanisms at the invading fronts of tumors remain largely unknown. Conflicting studies on the role of long noncoding RNA (lncRNA) MALAT1 (metastasis-associated lung adenocarcinoma transcript 1) in cancer metastasis highlight the complexity and challenges of revealing the dynamic functions of lncRNAs. This study introduces a nanobiosensor that monitors lncRNA dynamics in live single cancer cells and probes the spatiotemporal dynamics of lncRNAs at the invasion fronts of cancer cells and patient-derived spheroids. The findings demonstrate that lncRNA MALAT1 is dynamically regulated during collective cancer invasion, which could lead to the development of prognostic and therapeutic approaches targeting collective cancer invasion.

Author contributions: N.Z. and P.K.W. designed research; N.Z. and M.A. performed research; Y.L. and J.C.L. contributed new reagents/analytic tools; N.Z., M.A., Y.L., J.C.L., and P.K.W. analyzed data; and N.Z. and P.K.W. wrote the paper.

Competing interest statement: The authors declare that the research was conducted in the absence of any commercial or financialrelationships that could be construed as a potential conflict of interest.

This article is a PNAS Direct Submission.

[1]To whom correspondence may be addressed. Email: pak@engr.psu.edu.

This article contains supporting information online at https://www.pnas.org/lookup/suppl/doi:10.1073/pnas.2305410120/-/DCSupplemental.

Published June 26, 2023.

from muscle-invasive bladder cancer patients. The formation and termination of leader cells in invading tumor structures were characterized to investigate the function of MALAT1 in collective cancer invasion.

Results

Visualization of lncRNA in Live Cancer Cells with a Dual dsLNA Nanobiosensor. A nanobiosensor was developed to study the dynamics of lncRNAs in live cancer cells at the single-cell level. The nanobiosensor combines a dual probe design, dsLNA probes, and FRET-based sensing to improve the signal-to-noise ratio (31–34). The nanobiosensor comprises two pairs of dsLNA probes, each with a fluorophore sequence and a quencher sequence (Fig. 1*A*). The fluorophore-labeled LNA probes (donor and acceptor) are complementary to a specific, accessible region of the target lncRNA sequence. In the absence of the target molecule, the fluorophores of donor and acceptor probes are separated and quenched, resulting in a low background signal. However, when the target molecule is present, the quencher probes are displaced, and the donor and acceptor probes come in close proximity, allowing for efficient energy transfer from donor to acceptor, generating a strong FRET signal (*SI Appendix*, Fig. S1). The FRET approach reduces the background noise associated with autofluorescence and thermal dissociation of the quencher probe, facilitating detection of endogenous RNA transcripts in live single cells (Fig. 1*B* and *SI Appendix*, Fig. S2). The FRET signal was validated by transient knockdown with siRNA, RNA FISH, and TGF-β1 stimulation (*SI Appendix*, Figs. S3–S5). The nanobiosensor was applicable for detecting lncRNA expressions in migrating cell monolayers, patient-derived tumor spheroids, and 3D cancer spheroids (Fig. 1 *C*–*E* and Movie S1).

The expressions of β-actin, MALAT1, and UCA1 were measured in live bladder cancer cells (5,637). The RNA expressions were estimated by the fluorescent puncta in the FRET channel, which represent one or more RNA transcripts (Fig. 2 *A*–*C*). The nuclear and

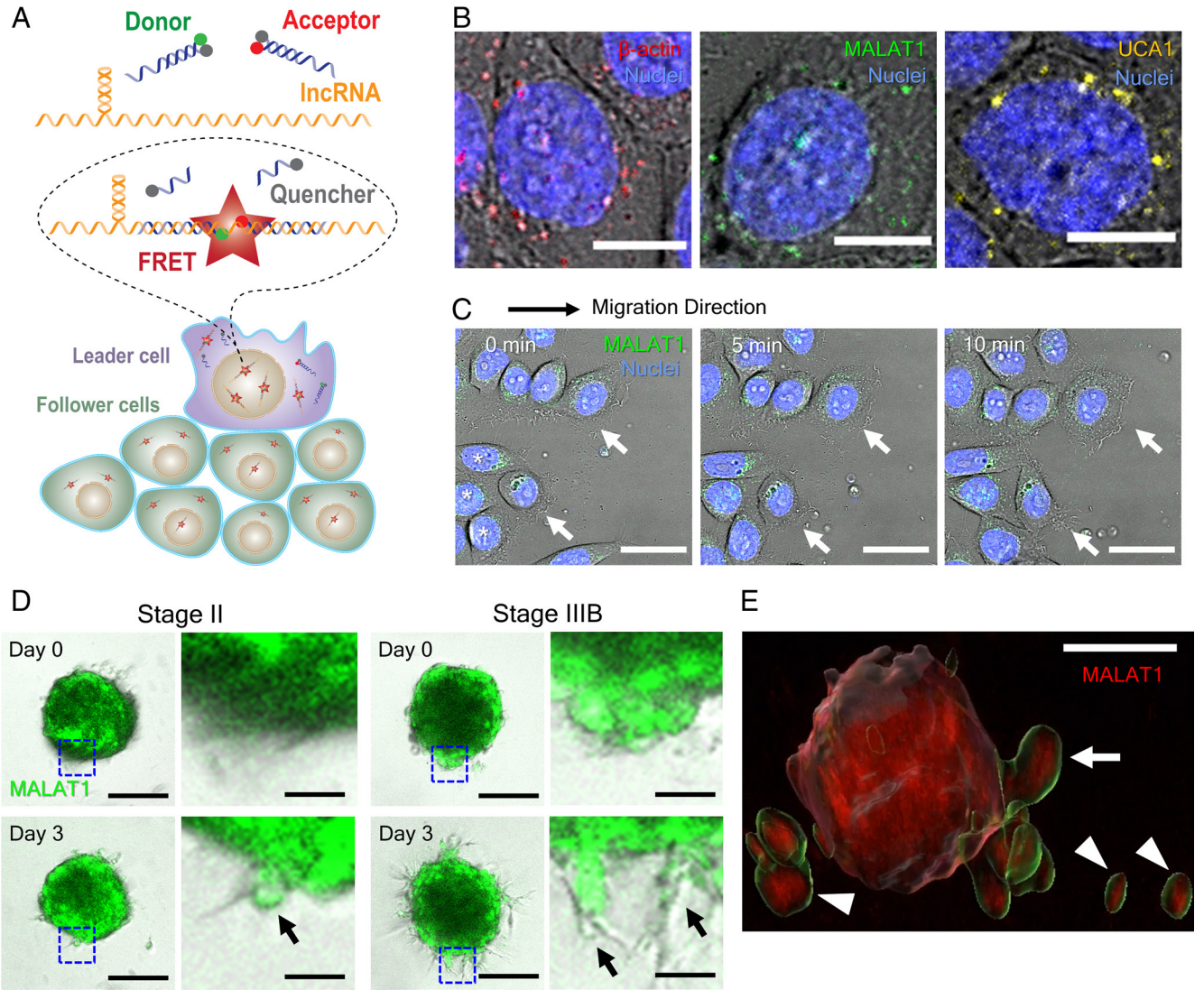

Fig. 1. A dual double-stranded LNA nanobiosensor for probing lncRNA dynamics during collective cancer invasion. (*A*), Schematics of the FRET-based LNA nanobiosensor for detecting lncRNA in leader and follower cells. (*B*), Intracellular distributions of β-actin, MALAT1, and UCA1 RNA expressions detected by the nanobiosensors in live cancer cells (5,637). (Scale bars, 10 μm.) Images are representative of eight experiments. (*C*), Time-lapse images for MALAT1 dynamics in leader cells (marked by white arrows) during collective cell migration. (Scale bars, 30 μm.) Images are representative of five experiments. (*D*), Detection of MALAT1 expression in 3D tumor spheroids derived from patients with muscle-invasive bladder cancer. Blue dashed squares indicate the zoom-in regions (*Right*). Black arrows indicate protruding structures with leader cells sprouting from the spheroids. [Scale bars, 200 μm (*Left*) and 40 μm (*Right*).] Images are representative of six (Stage II) and ten (Stage IIIB) tumor spheroids. (*E*), 3D rendering of a cancer spheroid with leader cells (white arrows) and dissociated cancer cells (white arrowheads). (Scale bar, 200 μm.)

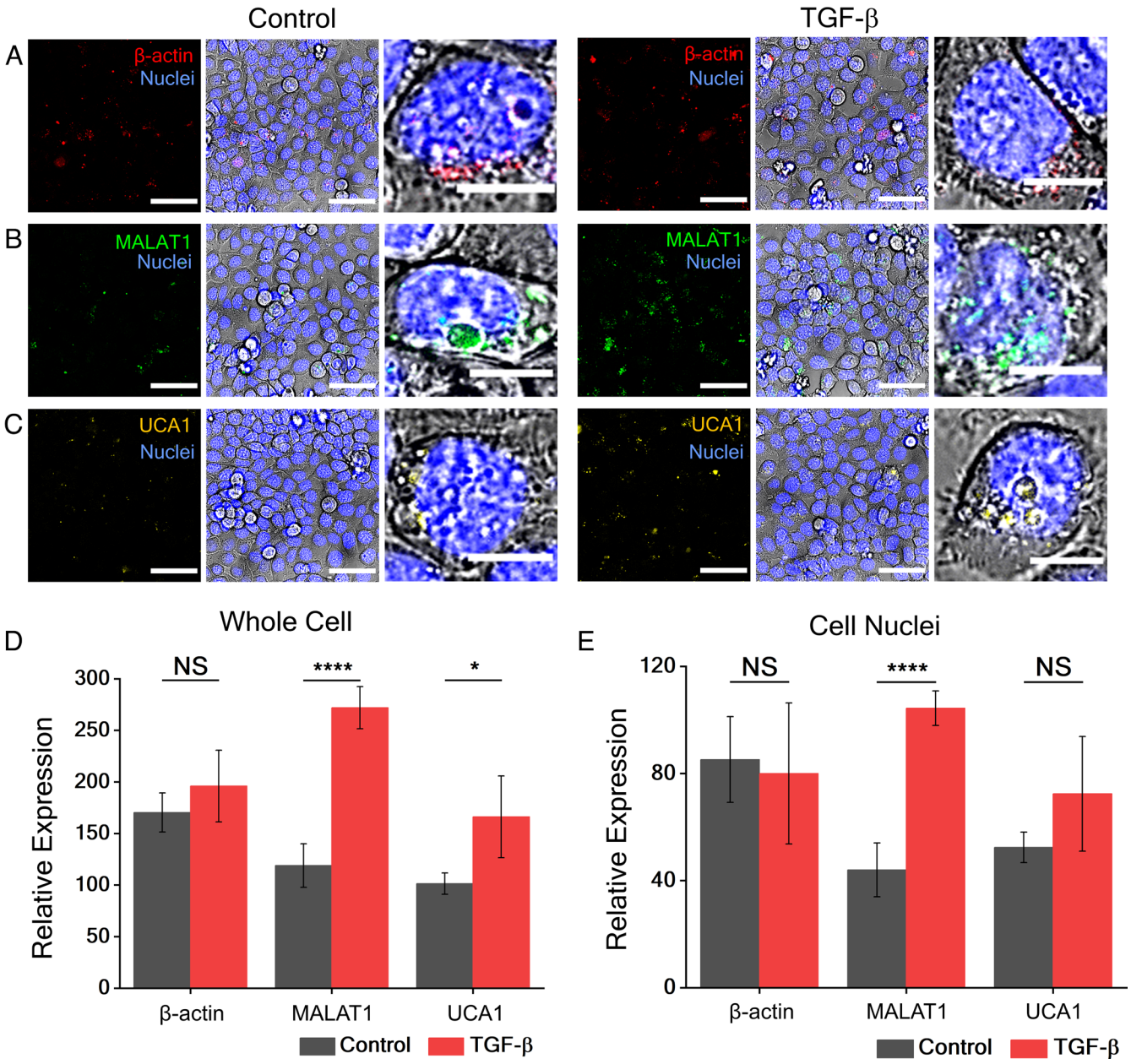

Fig. 2. LNA nanobiosensors detect TGF-β-induced MALAT1 upregulation in cell nuclei and cytoplasm. (*A–C*), Confocal images of β-actin mRNA, MALAT1, and UCA1 in live bladder cancer cells (5,637). The cells were treated with buffer control and TGF-β. FRET channels (*Left*), merged FRET and brightfield channels (*Middle*), and zoom-in views of single cells (*Right*) are shown to illustrate the expression distributions. Images are representative of five experiments. [Scale bars, 50 μm (*Left* and *Middle*), 10 μm (*Right*).] (*D* and *E*), Relative expression of β-actin, MALAT1, and UCA1 RNA (*D*) in whole cells and (*E*) colocalized with the nuclei. One-way ANOVA followed by Tukey's post hoc test was used to compare transcript numbers between control and TGF-β treatment (n = 5, NS not significant, $^*P < 0.05$, $^{****}P < 0.0001$).

cytoplasmic signals were examined to evaluate the distribution of RNA transcripts in live cells. A live-cell nuclear dye was applied to detect the colocalization of the RNA transcripts and the nuclei by confocal microscopy. The number of transcripts of β-actin, MALAT1, and UCA1 in the cytoplasm was generally higher than the number of the transcripts colocalized with the nucleus. With TGF-β treatment, which induces EMT (35), the total MALAT1 and UCA1 expressions were increased in the cells (Fig. 2*D*). A similar ratio of MALAT1 (but not UCA1) upregulation was observed in the nuclei (Fig. 2*E*). In contrast, the β-actin mRNA expression levels were not changed in the cytoplasmic and nuclear regions.

Analyzing the Abundance, Diffusivity, and Distribution of MALAT1 in Leader Cell during Collective Cell Migration. The scratch cell migration assay (also known as the wound healing assay) was applied to study the dynamics of lncRNA in collectively migrating bladder cancer cells (36). In agreement with previous studies (37, 38), the cancer cells migrated coherently and formed protruding tips with the leader–follower organization (Fig. 3*A*). The formation of migration tips and leader cells was clearly observed 8 h after scratching. In this study, the cells at the protruding tips were considered leader cells, and the cells behind were considered as follower cells. Notably, MALAT1 expression was significantly higher in leader cells compared to follower cells (Fig. 3*A*). On the other hand, β-actin mRNA and UCA1 expressions were comparable between leader cells and follower cells.

The functions of MALAT1 in collective cancer migration were further investigated by siRNA treatment (Fig. 3 *B* and *C*). Transient knockdown of MALAT1 abolished collective cell migration. The boundary of the monolayer retracted slightly and

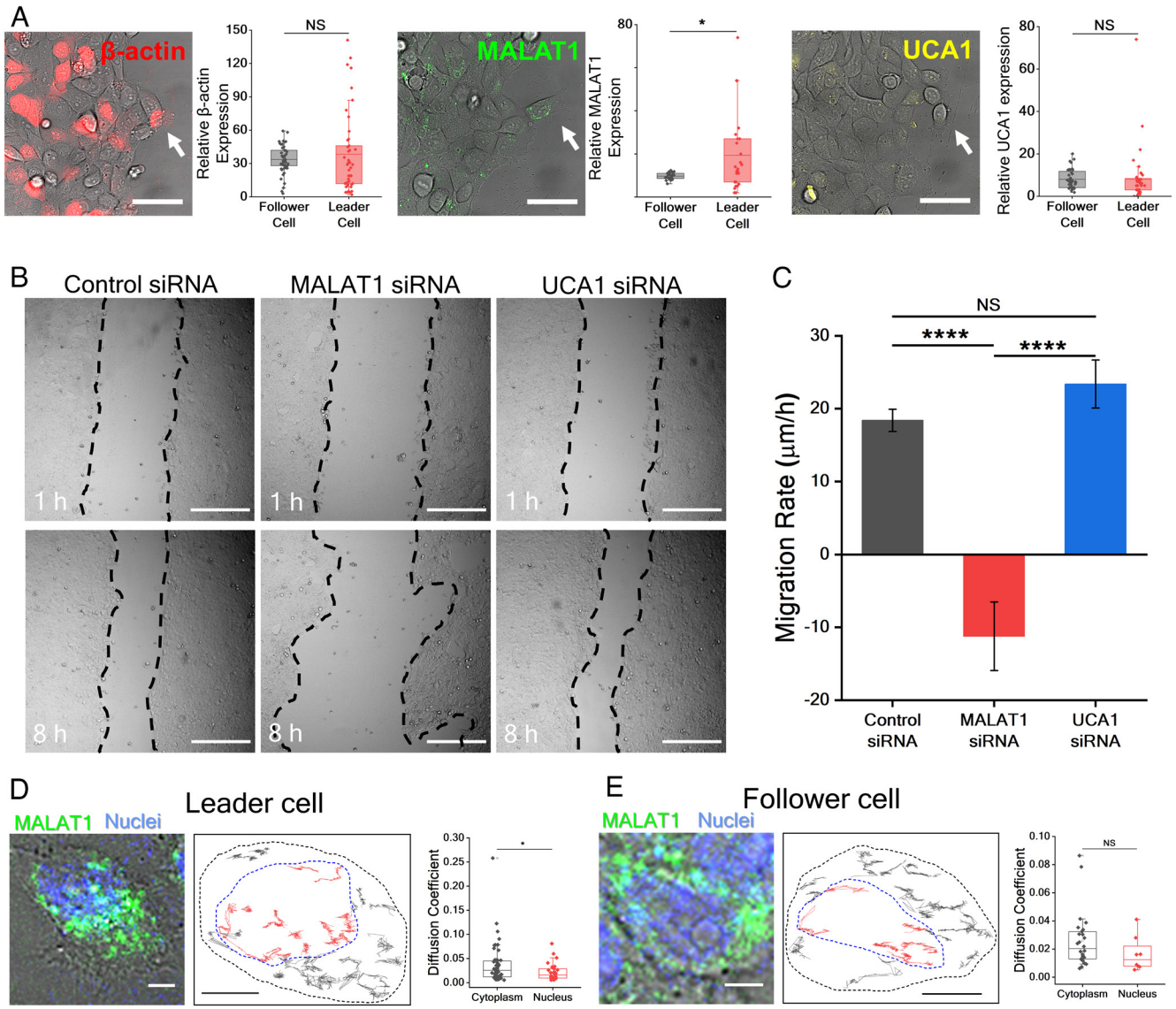

Fig. 3. MALAT1 is up-regulated in leader cells during collective cancer migration. (*A*), Detection of β-actin mRNA, MALAT1, and UCA1 in leader cells and follower cells. Collective cell migration was induced by scratching the cell monolayer. Cells at the protrusion tip with an aggressive morphology, exhibiting significant amount of lamellipodia and filopodia, are considered leader cells (white arrows), and cells behind the leader cells were considered follower cells. Images are representative of four experiments. (Scale bars, 50 μm.) Student's *t* test was used to compare the expression between the leader and follower cells (n ≥ 25, NS not significant, $*P < 0.05$). (*B*), Collective migration of cancer cells treated with control siRNA, MALAT1 siRNA, and UCA1 siRNA at 1 h and 8 h. Black dotted lines illustrate the boundary of the migrating cells. Images are representative of four experiments. (Scale bars, 300 μm.) (*C*), Cell migration rate estimated by the average distance between the cell boundaries. One-way ANOVA followed by Tukey's post hoc test was used to compare the migration rates (n = 4, NS not significant, $****P < 0.0001$). (*D* and *E*), Single-molecule tracking of MALAT1 transcripts in leader cells and follower cells. (*Left*) Representative images from eight experiments. (Scale bars, 5 μm.) (*Middle*) Traces of MALAT1 transcripts. Black and blue dashed lines indicate the cell boundary and the nucleus, respectively. (Scale bars, 5 μm.) (*Right*) Comparison of cytoplasmic and nuclear diffusivities of MALAT1. Student's *t* test was used to compare the diffusivities of MALAT1 RNA in the nucleus and cytoplasm (n ≥ 5, NS not significant, $*P < 0.05$).

resulted in a negative average migration rate. Examining the cell morphology revealed a nonmigratory phenotype. In contrast, downregulation of UCA1 did not display a substantial change in the cell morphology, and the migration rate was comparable to the control siRNA. We also treated the migrating monolayers with TGF-β (*SI Appendix*, Fig. S6). While coherent monolayers were observed in the control group, TGF-β treatment disrupted the cell–cell adhesion and dissociated cancer cells in the scratched monolayers.

We further examined MALAT1 dynamics in leader and follower cells by single-molecule tracking (Fig. 3 *D* and *E* and Movies S2 and S3). The mean squared displacement (MSD) and diffusivity of the molecules were estimated by tracking the position of MALAT1 transcripts as a function of time. We observed different distributions of MALAT1 diffusivity in leader and follower cells. In leader cells, MALAT1 in the cell nuclei exhibited a lower diffusivity compared to MALAT1 in the cytoplasm (Mann–Whitney test, $P = 0.0373$). In contrast, the MALAT1 diffusivity in follower cells was similar between the nuclei and cytoplasm (Mann–Whitney test, $P = 0.0639$). The distinct behaviors of MALAT1 in leader and follower cells were also supported by considering anomalous diffusion, where $MSD = 4Dt^{\alpha}$ (*SI Appendix*, Fig. S7). We observed the power exponent, α, distributed from 0 to 2.5 in leader and follower cells. The values could be clustered into groups with high and low alpha ($\alpha > \text{or} < 0.6$). The portion of MALAT1 transcripts with a low power exponent was higher in leader cells (Chi-Square test, $P = 0.0007$). The differences in abundance, diffusivity, and distribution suggest that MALAT1 in leader cells

may engage in different molecular complexes and activities compared to follower cells during collective cancer migration.

Dynamics of MALAT1 in Leader Cells during 3D Collective Invasion. We then evaluated the relationship between MALAT1 and leader cells using a 3D tumor invasion assay (34, 38). We formed 3D cancer spheroids with bladder cancer cells transfected with the dual dsLNA nanobiosensor. The nanobiosensor was transfected into the cells before spheroid formation to ensure uniformity of probe transfection. The tumor spheroids were embedded in an invasion matrix consisting of collagen I and basement membrane extract, representing the lamina propria and basement membrane compositions. TGF-β was added to the invasion matrix to induce invasion. The cancer spheroids were allowed to invade for a period of 3 d (Fig. 4*A* and *SI Appendix*, Fig. S8). Protruding cells were observed in approximately 24 h. The sprouting structures continued to grow and invaded into the invasion matrix. Examining the spatial distribution revealed that MALAT expression was up-regulated at the outer region of the spheroid, where the cancer cells interfaced with the invasion matrix. Interestingly, as the sprouts continued

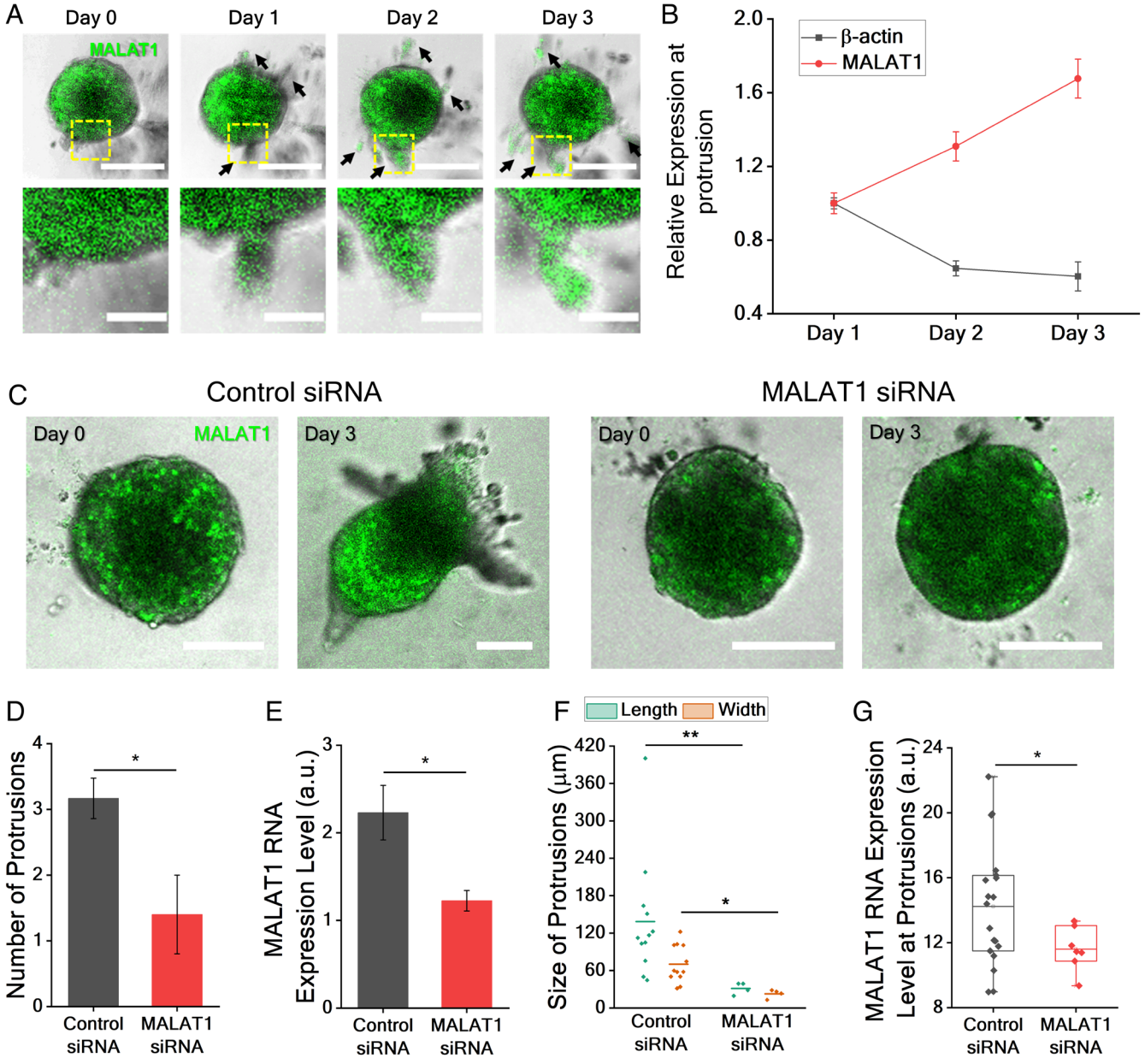

Fig. 4. MALAT1 is up-regulated in invading sprouts of 3D bladder cancer spheroids. (*A*), Bladder cancer spheroids (5,637) were treated with TGF-β (40 ng/mL) and allowed to invade the invasion matrix for 3 d. Black arrows indicate invading protrusions from the spheroid. Yellow dashed squares highlight a protruding structure in the zoom-in views (*Bottom*). [Scale bars, 250 μm (*Top*) and 80 μm (*Bottom*).] Images are representative of five experiments. (*B*), The expression of β-actin mRNA and MALAT1 at protrusions. The value was normalized to the initial intensity. One-way ANOVA was used to analyze the RNA expression level, indicating an increasing MALAT1 expression ($P = 5.82 \times 10^{-5}$) and a decreasing β-actin expression ($P = 0.0023$) (n ≥ 3). (*C*), MALAT1 siRNA and control siRNA treated spheroids in the 3D invasion assay. (Scale bars, 150 μm.) Images are representative of three experiments. (*D*), Comparison of the number of protrusions per spheroid with control siRNA and MALAT1 siRNA on day 3. (*E*), Comparison of MALAT1 expression of cancer spheroids with control and MALAT1 siRNA. Student's *t* test was used to compare the number of protrusions and the MALAT1 expression (n = 6 for control siRNA and n = 5 for MALAT1 siRNA, $^*P < 0.05$). (*F*), The length and width of protrusions from the cancer spheroids on day 3. Two-way ANOVA followed by Tukey's post hoc test was used to compare the dimensions of protrusions from spheroids with MALAT1 siRNA and control siRNA (n = 4 for MALAT1 siRNA and n = 12 for control siRNA, $^*P < 0.05$, $^{**}P < 0.01$). (*G*), MALAT1 expression at the protrusions of spheroids treated with MALAT1 siRNA and control siRNA on day 3. Student's *t* test was used to compare the expression. (n = 7 for MALAT1 siRNA and n = 19 for control siRNA, $^*P < 0.05$).

to invade the matrix, the MALAT1 expression of the sprouts also increased during the 3-d invasion period. As a control, β-actin mRNA decreased slightly in the same period (Fig. 4*B*).

To investigate the role of MALAT1 in 3D collective cancer invasion, we knocked down MALAT1 by siRNA (Fig. 4*C*). Similar to the 2D experiment, the formation of invasive sprouts and leader cells was attenuated by MALAT1 siRNA (Fig. 4*D*). The nanobiosensor revealed that the cancer spheroids with MALAT1 siRNA had a lower MALAT1 expression level (Fig. 4*E*). The length and width of the protrusions from the cancer spheroids were decreased in the MALAT1 siRNA group (Fig. 4*F* and *SI Appendix*, Fig. S9). Therefore, both the amount of leader cells and follower cells were reduced. In control and MALAT1 siRNA, MALAT1 was up-regulated near the outer surface of the spheroids. At the protrusions, the MALAT1 expression was reduced in the MALAT1 siRNA group compared to the control group (Fig. 4*G*). These results support the notion that MALAT1 is associated with the formation of leader cells and collective invasion in 3D microenvironments.

MALAT1 Is Up-Regulated in Patient-Derived Cancer Cells. We evaluated the involvement of MALAT1 in patient-derived cancer cells and tumor spheroids (39). Single-cell analysis with the dual dsLNA nanobiosensor revealed that MALAT1 was heterogeneous among the cancer cells. Specifically, a subset (5 to 10%) of cells expressed a high level of MALAT1 that was visually distinct from the rest of the population (Fig. 5*A*). The heterogeneity could not be explained by the transfection efficiency between the primary cancer cells, as transfection was effective and relatively uniform for detecting β-actin mRNA. We analyzed the MALAT1 expression and estimated the portion of MALAT1-expressing cells (Fig. 5 *B*–*D*). The MALAT1 expression in the stage IIIB sample was significantly higher than the value in the stage II sample. In contrast, the β-actin mRNA expressions were similar in the samples. Nevertheless, the portions of MALAT1 cells were similar between the stage II and stage IIIB samples, suggesting the increase was mainly contributed by an enhanced MALAT1 expression instead of the portion of MALAT1-expressing cells.

Patient-derived primary cancer cells were also studied using the scratch cell migration assay (*SI Appendix*, Fig. S10). However, the cell monolayer was less coherent compared to typical epithelia in wound healing studies (38, 40). After scratching, the cells exhibited an elongated, spindle-shaped, or mesenchymal-like, morphology near the migrating front. While leader–follower organization could still be observed in some cases, the cells were not physically aligned, suggesting a weak physical interaction. Furthermore, we did not observe a substantial change in the number of MALAT1-expressing cells. MALAT1 expression was randomly expressed in leader and follower cells in the loose monolayer.

MALAT1 Is Associated with Leader Cells in Patient-Derived Tumor Spheroids. We investigated the function of MALAT1 by generating tumor spheroids in the 3D invasion assay (Fig. 6 *A*–*G* and *SI Appendix*, Fig. S11). The cancer cells were dissociated from tumor samples derived from patients with muscle-invasive bladder cancer including stage II, IIIA, IIIB, and IV. Examining the spheroids revealed the samples disseminated as collectively invading sprouts with leader cells or detached individual cells (Fig. 6 *H* and *I*). The stage II samples exhibited a relatively low number of invading cells. However, the clinical stage did not directly correlate with the number of leader cells and detached cells. For instance, a stage IIIA sample (DT2148) engaged in both detached cells and protruding structures with the leader–follower organization while a stage IIIB sample (DT2153) exhibited invading sprouts with apparent filopodial structures and relatively less detached cells. For the stage IV sample (DT2296), there were many detached cells, and the protrusions showed a loose, irregular morphology. Therefore, the patient-derived tumor spheroids appeared to utilize one or more invasion modes (1).

To examine the relationship between MALAT1 in the invasive modes, we examined the expression of MALAT1 in these samples. For all patient-derived samples tested, MALAT1 was strongly expressed at the surface of the tumor spheroids. The MALAT1 expression was measured in the detached cells and invading sprouts. We first evaluated the relationship of MALAT1 with the volume of the invading sprouts and clinical stage (Fig. 6*J* and *SI Appendix*, Figs. S12 and S13). The sprout volume and clinical stage displayed only a weak correlation with MALAT1 (adjusted R-square 0.30). In contrast, the detached cells per spheroid displayed a negative relationship (adjusted R-square 0.65) with the

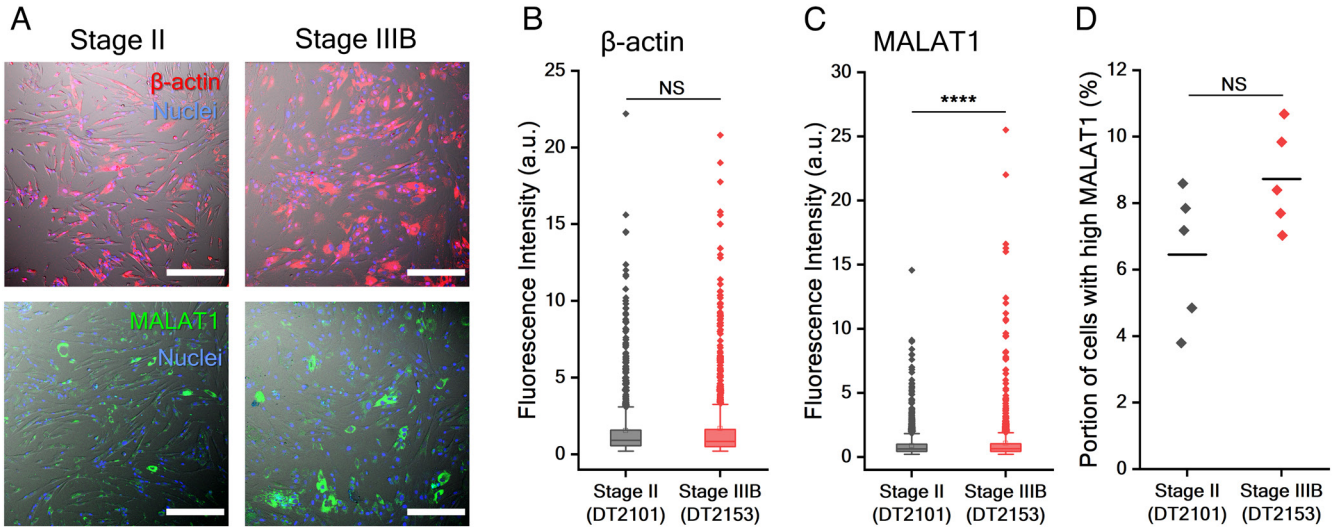

Fig. 5. MALAT1 expression is associated with the clinical stage of bladder cancer patient-derived cancer cells. (*A*), β-actin mRNA and MALAT1 expressions in cancer cells derived from bladder cancer patients. (Scale bars, 300 μm.) (*B* and *C*), MALAT1 is up-regulated in the stage IIIB sample compared to the stage II sample. (*D*), The portion of cells with a high level of MALAT1. Student's *t* test was used to compare between samples (n ≥ 1,148 for gene expression and n = 5 for cell portions with an enhanced MALAT1 expression).

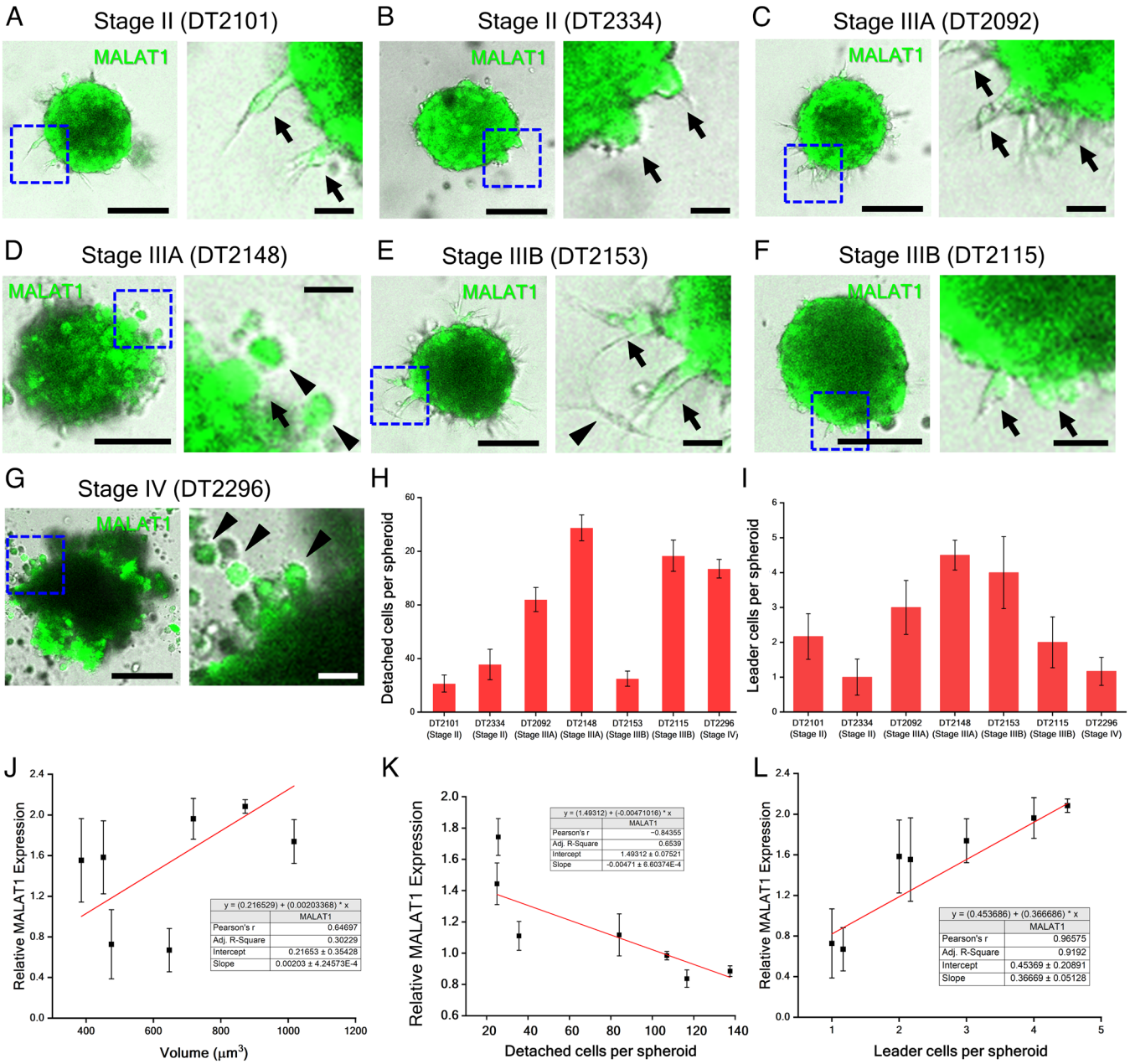

Fig. 6. MALAT1 is associated with leader cells in tumor spheroids derived from muscle-invasive bladder cancer patients. (*A–G*), MALAT1 expression in 3D human tumor spheroids derived from bladder cancer patients. Clinical samples of stage II (DT2101 and DT2334), Stage IIIA (DT2092 and DT2148), Stage III (DT2153 and DT2115), and Stage IV (DT2296) were included to cover the spectrum of muscle-invasive bladder cancer. Blue dashed squares highlight the zoom-in views (*Bottom*) with leader cells (black arrows) or dissociated cells (black arrowheads). [Scale bars, 200 μm (*Top*) and 100 μm (*Bottom*).] Images are representative of at least six spheroids. (*H* and *I*), The number of detached cells and protrusions per spheroid on day 3 (n = 5). (*J–L*), Correlation of the spheroid volume, the number of detached cells, and the number of leader cells with MALAT1 expression on day 3. At least five spheroids were analyzed for each sample, and all detectable leader cells and detached cells were analyzed.

MALAT1 expression in the detached cells (Fig. 6*K*). Most importantly, the MALAT1 expression in leader cells increased linearly (adjusted R-square 0.92) with the number of sprouts per spheroid (Fig. 6*L*). Overall, the tumor spheroid results further supported the notion that MALAT1 is associated with the coordination of leader cells during collective cancer invasion.

Real-Time Dynamics of lncRNA in Leader Cells. Since our results suggest MALAT1 expression is associated with cell coordination, we performed single-cell tracking experiments during collective cancer migration. Time-lapse images of the migrating monolayer were taken near the leading edges during cell migration and closure of the monolayer (Fig. 7*A* and Movie S4). The expressions of MALAT1 were dynamically monitored in cells near the migrating front. The nuclear MALAT1 transcript was analyzed to study the MALAT1 intracellular distribution and compare with the cell behaviors. Fig. 7*B* shows leader cell switching and termination during collective cell migration (Movie S5 and *SI Appendix*, Fig. S14). A follower cell (marked by yellow dashed lines) migrated to the leading edge (0 to 30 min) and took over the leader cell position. The cell also acquired an aggressive morphology with active lamellipodia (30 to 60 min). The newly formed leader cell led follower cells and merged with the other leading edge. The leader cells contacted the other leading edge at 70 min (i.e., the cell-contact time), and the edges continued to merge (120 min). Remarkably, the portion of nuclear MALAT1 strongly correlated

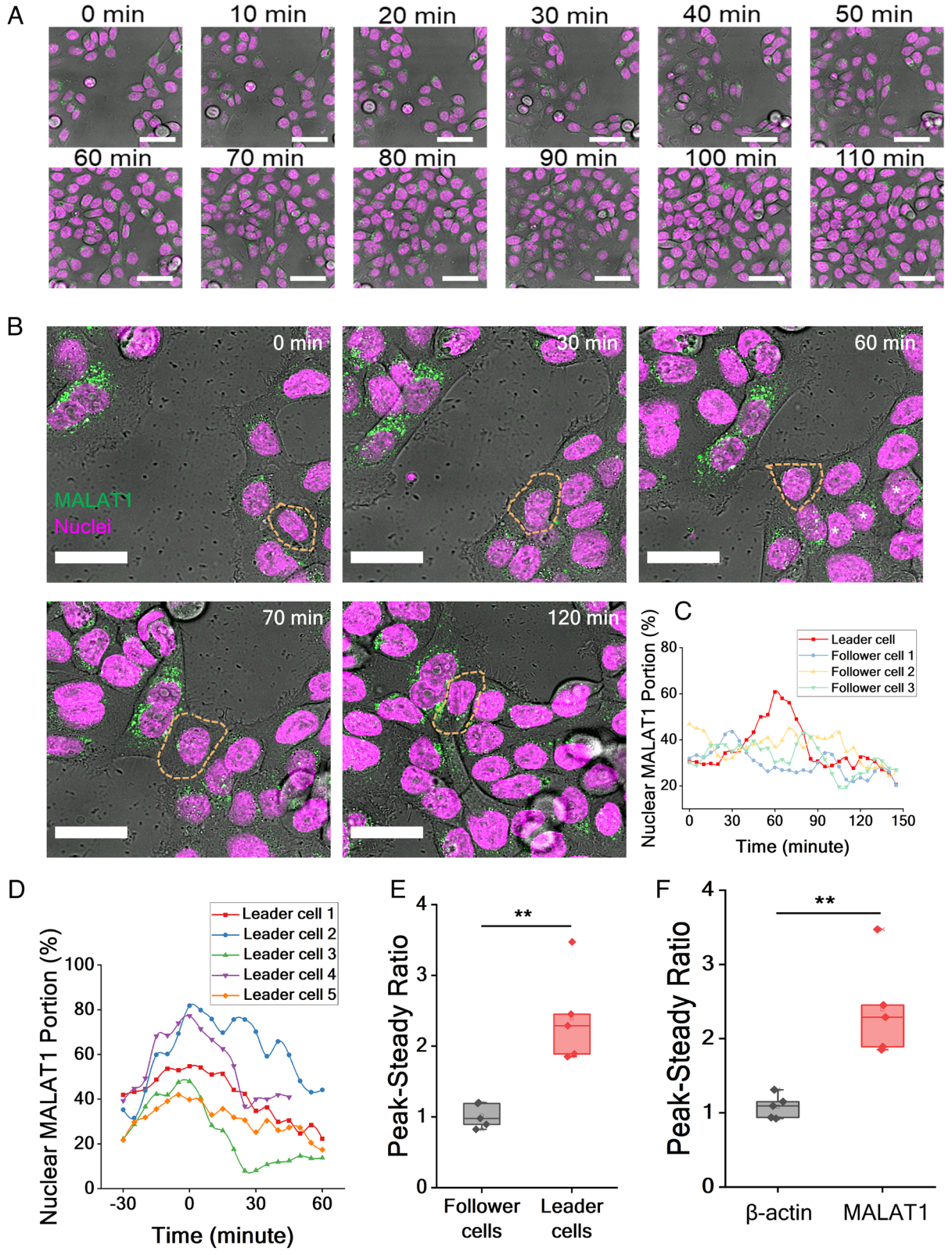

Fig. 7. MALAT1 is dynamically regulated during the formation and termination of leader cells. (*A*), Time lapse images of cancer cells (5673) during collective cell migration induced by the scratch assay. (Scale bars, 50 μm.) (*B*), Time-lapse images tracking the switching and termination of a leader cell (yellow dashes) near the migrating front. A follower cell was initially behind the cell boundary. The cell migrated to the front, acquired the leader cell role, and displayed an aggressive morphology. Then, the leader cell reached the other boundary and was surrounded by other cells in the monolayer. (Scale bars, 20 μm.) (*C*), Tracking of nuclear MALAT1 of the leader cell and follower cells outlined in (*B*). Data represent the portion of nuclear MALAT1 in the cell. MALAT1 increased when the cell assumed the role of leader cell and decreased when the boundary merged. (*D*), Examples of nuclear MALAT1 in leader cells during the merging of cell boundaries. Time zero (or peak) is when the leader cells reached and contacted the other boundary. MALAT1 returned to the basal level (or steady state) in 30 to 60 min. (*E*), Peak-steady ratio of nuclear MALAT1 in leader cells and follower cells. (*F*), Peak-steady ratio of nuclear MALAT1 and β-actin mRNA in leader cells. Student's *t* test was used to compare the Peak-steady ratio (n = 5, $^{**}P < 0.01$).

with the position of the cells (Fig. 7*C*). In particular, the nuclear MALAT1 remained steady at the basal level (~30%) from 0 to 30 min when the cell was in the follower position. From 30 to 60 min, when the cell took over the leader position and exhibited an aggressive morphology, the nuclear MALAT1 increased from 30% to over 60%. From 60 min to 120 min, when the leading edges merged to form a monolayer, the nuclear MALAT1 returned to the basal level gradually (most rapidly between 60 and 90 min).

We further analyzed leader cell behaviors during other cases of cell monolayer closure. When the cell-contact time was considered as time zero, a similar pattern of the nuclear MALAT1 was generally observed in leader cells (Fig. 7*D*). The nuclear MALAT1 in leader cells dropped approximately 50 to 60% (or a peak-steady ratio of >2) from the peak value (Fig. 7*E*). In contrast, the nuclear MALAT1 maintained constant (i.e., a peak-steady ratio of ~1) in follower cells (Fig. 7*E*). Furthermore, the change in the nuclear MALAT1 was not observed in β-actin mRNA of leader cells (Fig. 7*F*). These observations collectively supported the notion that MALAT1 is dynamically regulated in leader cells during collective cancer invasion.

Discussion

In this study, we show a dual dsLNA nanobiosensor for probing lncRNA dynamics in live single cells. By combining single-cell and single-molecule tracking techniques, we demonstrate spatiotemporal analysis of lncRNA during collective cancer invasion, which is challenging for conventional RNA detection techniques. The dual dsLNA nanobiosensor has several advantages and disadvantages compared to other live-cell RNA-sensing techniques (25, 26). First, the nanobiosensor detects endogenous RNA transcripts and is compatible with both 2D collective cell migration and 3D cancer invasion models. This enables the detection of lncRNAs in patient-derived cancer cells and tumor spheroids. Second, the combination of LNA modification, the double-stranded probe, and the FRET dual probe design provides outstanding stability, sensitivity, and signal-to-noise ratio for tracking lncRNA in live cells. The ability of tracking endogenous RNA transcripts allows the monitoring the abundance, diffusivity, and distribution, facilitating the study of the diverse modes of action of lncRNA (11–13). Nevertheless, the capability of detecting multiple lncRNA targets is limited by the spectrum overlapping from donor and acceptor probes of FRET. Future studies may combine the nanobiosensors and single-cell sequencing techniques to detect a larger number of RNA.

Our results reveal that MALAT1 is associated with collective invasion of muscle-invasive bladder cancer. MALAT1 expression was up-regulated in leader cells and correlated with the aggressiveness of cancer cells. Attenuating MALAT1 disrupted collective cancer migration and reduced the formation of invading sprouts in the 3D invasion assay. As demonstrated in tumor spheroids derived from patients with muscle-invasive bladder cancer, the invasiveness of the samples, indicated either by the number of sprouts or the number of detached cells in the 3D invasion matrix, increased with the tumor stage. Interestingly, MALAT1 correlated positively with the formation of leader cells and invading protrusions (ANOVA, $P = 4.094 \times 10^{-4}$) but negatively with the detached individual cells (ANOVA, $P = 0.0171$), supporting its association with collective cancer invasion. Thus, the combination of the spheroid invasion assay and the nanobiosensor targeting MALAT1 may provide a diagnostic approach for identifying the invasion mode of muscle-invasive bladder cancer. Future clinical studies with additional patient-derived tumor samples (e.g., from transurethral resection of bladder tumor) and detection techniques are warranted for validating the translational potential of MALAT1 in bladder cancer prognosis.

Our study suggests that MALAT1 is dynamically regulated in leader cells. The mechanistic interactions between MALAT1 and leader cells have not been established. Previous studies suggest that MALAT1 modulates gene expression and interacts with various transcription factors (e.g., TEAD), microRNAs (e.g., miR200 and miR-125b), splicing factors (e.g., SR proteins), and epigenetic regulators (e.g., EZH2) (16). In particular, MALAT1 has been reported to modulate EMT by sponging miRNA (miR200 and miR125b) and inhibiting Ezh2-Notch1 signaling (20, 41–43). In agreement, we observed upregulation of MALAT1 with TGF-β in 5,637 cells. The cells exhibited aggressive mesenchymal-like morphology, and MALAT1 transcripts were enhanced in the nuclei after TGF-β treatment. MALAT1 expression was also increased near the migrating front in the scratch cell migration assay (36) and TGF-β-induced 3D invasion (35). The single-molecule tracking feature of the nanobiosensor also revealed a decrease in diffusivity of MALAT1 in the nuclear of leader cells. Furthermore, our recent study revealed that collective invasion and leader cell formation can be spatially coordinated by the Nrf2-EMT-Notch1 circuit (38). The function of MALAT1 in modulating EMT may provide a mechanism for regulating the formation of leader cells. Moreover, MALAT1 is known to regulate cell–cell and cell–matrix interactions through the Hippo-YAP/TEAD signaling (43, 44). As observed in the single-cell tracking experiments, MALAT1 increased when a cell took over the leader position and when an invading sprout penetrated the 3D invasion matrix. In contrast, MALAT1 was down-regulated when leader cells were in contact with other cells during the closure of the monolayer, and disruption of MALAT1 abolished the collective cancer invasion. These observations support that MALAT1 may be associated with cell interactions with the environment and neighboring cells, which are major functions of leader cells (2). Future studies with other molecular characterization techniques, specific gene editing approaches, systems biological computational analysis, and physiologically relevant models will be required to elucidate the molecular mechanisms and functions of MALAT1 in leader cell formation and cancer invasion.

Taken together, this study demonstrates a dual dsLNA nanobiosensor with a high spatiotemporal resolution for investigating lncRNA dynamics in live single cells. Using the nanobiosensor, our results suggest a role of MALAT1 in the dynamic regulation of leader cells during collective cancer invasion. The finding may create opportunities in developing prognostic and therapeutic approaches for cancer in the future.

Materials and Methods

Cell Culture and Reagents. The human bladder cancer cell line 5,637 from American Type Culture Collection (Manassas, VA) was cultured in RPMI 1640 medium supplemented with 10% fetal bovine serum and 10 mg/mL Gentamicin (Fisher Scientific, Hampton, NH). The human bladder cancer dissociated tumor cells (stage II, lot number: DT02101 and DT02334; stage IIIB, lot number: DT02153; stage IV, lot number: DT02296) purchased from BioIVT (Westbury, NY) were cultured in Dulbecco's Modified Eagle's Medium (DMEM; Fisher Scientific, Hampton, NH) supplemented with 10% fetal bovine serum and 10 mg/mL Gentamicin. The cells were cultured at 37 °C in a humidified incubator with 5% CO_2 and seeded in 24-well glass bottom plates (Cellvis; Mountain View, CA) 24 h prior to experiments.

The MALAT1 siRNA (Silencer® Select, Catalog #: 4392420), UCA1 siRNA (Silencer® Select, Catalog #: 4392420) and control siRNA (Silencer® Select Negative Control No. 1 siRNA, Catalog #: 4390843) were purchased from Thermo Fisher Scientific (Waltham, MA). To knockdown MALAT1 and UCA1 expressions, 20 nm siRNAs were transfected into the cells by Lipofectamine RNAiMAX according to the

manufacturer's protocol (Fisher Scientific, Hampton, NH) for 48 h. To modulate MALAT1 and UCA1 expressions, transforming growth factor beta 1 (TGF-β1; Bio-Techne, Minneapolis, MN) was added to the cells with a 10 ng/mL concentration for 48 h. Cell nuclei were stained by NucSpot® Live 650 Nuclear Stains (Biotium, Fremont, CA) for 10 min according to the manufacturer's protocol. Other reagents were purchased from Fisher Scientific (Hampton, NH) unless specified otherwise.

FRET Nanobiosensor Design and Probe Transfection. Dual double-stranded locked nucleic acid (dsLNA) probes and synthetic targets were synthesized by Integrated DNA Technologies (San Diego, CA). The FRET nanobiosensor consists of two dsLNA probes, modified with a donor and an acceptor (ATTO488-Cy3 or FAM-Texas Red). The fluorophores were labeled at 5′ end of the donor and 3′ end of the acceptor (*SI Appendix*, Tables S1–S3). The secondary structures of the lncRNAs were predicted by the mfold web server (http://www.unafold.org/) (45) to determine the accessible region (i.e., loops) of the lncRNA. The dual probes target two adjacent sequences (separated by four nucleotides) in an accessible region of the target lncRNA. The probes were designed to be in close proximity while preventing steric hindrance. A quencher probe was designed for each fluorescence probe to silence the unbound probes and enhance the signal-to-noise ratio. All sequences were aligned to the human transcriptome by the NCBI Basic Local Alignment Search Tool to verify and avoid binding to nonspecific RNAs.

The fluorophore and quencher probes were dissolved in sodium chloride-tris-EDTA (10 m tris, 1 m EDTA, and 100 m NaCl) and were mixed at a 1:3 ratio. The probes were then incubated at 37 °C for 15 min to form dsLNA. The FRET-based biosensor consists of a donor dsLNA and an acceptor dsLNA mixed at a 1:4 ratio. Then, the FRET-based biosensor was transfected into the cells cultured in 24-well glass bottom plates by Lipofectamine 3000 according to the manufacturer's protocol (Fisher Scientific, Hampton, NH). The final concentration of the donor probe in each well was 20 n. The cells were incubated with the biosensor for 24 h, followed by rinsing three times with 1× phosphate-buffered saline (PBS).

Cell Migration Assay. A scratch cell migration assay was performed to study collective cell migration. After reaching 100% confluency, the cell monolayer was scratched using a sterilized 200-mL pipet tip to create a cell-free region. The cell monolayer was rinsed with 1× PBS before and after scratching. The scratched cell monolayers were allowed to migrate and were imaged after 8 h. The distance between the two leading edges (wound width) was measured by Fiji ImageJ, and the migration rate was calculated by the difference of the initial and final wound width divided by migration time.

3D Invasion Assay and Patient-Derived Spheroids. A 3D invasion assay was applied to investigate the lncRNA dynamics in collective cancer invasion with Cultrex© 3D Spheroid Cell Invasion Assay Kits according to the manufacturer's instructions (R&D Systems, Minneapolis, MN). Briefly, bladder cancer cell line 5,637 or the human bladder cancer-dissociated tumor cells with the biosensor were incubated in Spheroid Formation Extracellular Matrix in a 96-well round bottom plate (10,000 cells per cell) for 3 d to form spheroids. The Invasion Matrix, consisting of collagen I and basement membrane extract, was added to the spheroids. After gel formation for an hour, fresh culture media were added. The spheroids were then imaged at 0, 24, 48, and 72 h.

Image Acquisition and Data Analysis. Images were obtained with a laser scanning confocal microscope (Leica TCS SP8; Leica Microsystems, Wetzlar, Germany) with an enclosed incubator (OKOlab, Italy) for temperature, humidity, and gas control. The donor probes were excited with a 488-nm solid-state laser, the acceptor probes were excited with a 514-nm (Cy3) or 552-nm (Texas Red) solid-state laser, and the cell nuclei stain was excited with a 638-nm solid-state laser. The fluorescence signals were collected with an NA = 0.9, 63× air objective. The fluorescence signals acquired from the wavelength 500 nm to 530 nm were determined as donor channel (excited with 488 nm laser) and the fluorescence signals acquired from the wavelength 530 nm (Cy3) or 570 nm (Texas Red) to 630 nm were determined as FRET channel (excited with 488-nm laser) and acceptor channel (excited with 514-nm or 552-nm laser).

For 2D monolayer experiments, a MATLAB (MathWorks, R2021a) program was developed to segment and quantify the puncta from the FRET channel of fluorescence images. The FRET channel images were binarized with a threshold of 0.02, and the number of connected components with size between 2 and 8 pixels (5.54 pixel/mm) was counted. The number of the puncta per cell was used to estimate the relative abundance of RNA and the portion of nuclear RNA. Images were processed by Fiji ImageJ.

For single-molecule tracking, the fluorescence signal from the biosensor, representing the RNA molecule, was captured at a frame rate of 1 Hz for 5 min. The tracking of transcripts was processed with Fiji ImageJ plugin "TrackMate". The DoG (differences of gaussian) detector was applied to identify the single particles with an estimated object diameter of 1.5 mm and quality threshold of 0.2. The Linear Assignment Problem tracker was applied to detect the trajectory of each single particle. To link the particles from frame to frame, the maximum distance was set to be 1 mm. The track segments were connected when the maximum distance of 2 mm and the maximum of two gaps were allowed for each track. The artifactual tracks were filtered by discarding the tracks with less than 60 particles per track and track mean speed higher than 1.37 mm/s. To interpret the single transcript tracking, the MSD of each track was calculated by $MSD(\Delta t) = \frac{1}{N}\sum_{i=1}^{N-\Delta t}\left[\left(x(t_i+\Delta t)-x\left(t_i\right)\right)^2+\left(y(t_i+\Delta t)-y\left(t_i\right)\right)^2\right]$ where N is the total number of particles in the track, Δt is the time interval (increment of 1 s), and $x(t_i)$ and $y(t_i)$ represent the position of the particle at frame i. The MSD was then modeled by anomalous diffusion, described by $MSD = 4Dt^{\alpha}$, where D is the diffusion coefficient, t is the time, and α is the exponent (46, 47). The diffusion coefficient of each track was acquired by the MATLAB curve fitting function.

The 3D spheroid images were analyzed by Imaris (Bitplane Inc., version 9.8). The 3D spheroids were rendered and segmented from the FRET channel of the z-stack images, and the lncRNA expression was determined by the mean fluorescence intensity.

Statistical Analysis. Data obtained from Fiji ImageJ, MATLAB and Imaris were analyzed with Origin software (OriginLab, version 9.9) and presented as mean ±SEM. All experiments were performed at least three times. Student's *t* tests were used to compare two experimental groups. One-way or two-way ANOVA followed by Tukey's post hoc test was used to compare multiple experimental groups. The statistical significance was symbolized by NS ($P > 0.05$), *($P \le 0.05$), **($P \le 0.01$), ***($P \le 0.001$), or ****($P \le 0.0001$).

Data, and materials Availability. All study data are included in the article and/or supporting information

ACKNOWLEDGMENTS. We thank Ian Eder and Sam Vilchez for technical support of the 3D invasion assay. This work was supported by the following funding. NSF: 1802947. NSF: 2033673. NIH: R21AR079095.

Author affiliations: [a]Department of Biomedical Engineering, The Pennsylvania State University, University Park, PA 16802; [b]Department of Electrical Engineering, The Pennsylvania State University, University Park, PA 16802; [c]Department of Urology, Stanford University School of Medicine, Stanford, CA 94305; [d]Department of Mechanical Engineering, The Pennsylvania State University, University Park, PA 16802; and [e]Department of Surgery, The Pennsylvania State University, University Park, PA 17033

1. P. Friedl, J. Locker, E. Sahai, J. E. Segall, Classifying collective cancer cell invasion. *Nat. Cell Biol.* **14**, 777–783 (2012).
2. S. A. Vilchez Mercedes *et al.*, Decoding leader cells in collective cancer invasion. *Nat. Rev. Cancer* **21**, 592–604 (2021).
3. K. Wolf, P. Friedl, Extracellular matrix determinants of proteolytic and non-proteolytic cell migration. *Trends. Cell Biol.* **21**, 736–744 (2011).
4. E. L. Zoeller *et al.*, Genetic heterogeneity within collective invasion packs drives leader and follower cell phenotypes. *J. Cell Sci.* **132**, jcs231514 (2019).
5. J. M. Westcott *et al.*, An epigenetically distinct breast cancer cell subpopulation promotes collective invasion. *J. Clin. Invest.* **125**, 1927–1943 (2015).
6. C. Gaggioli *et al.*, Fibroblast-led collective invasion of carcinoma cells with differing roles for RhoGTPases in leading and following cells. *Nat. Cell Biol.* **9**, 1392–1400 (2007).
7. J. Zhang *et al.*, Energetic regulation of coordinated leader-follower dynamics during collective invasion of breast cancer cells. *Proc. Natl. Acad. Sci. U.S.A.* **116**, 7867–7872 (2019).
8. R. Riahi *et al.*, Notch1–Dll4 signalling and mechanical force regulate leader cell formation during collective cell migration. *Nat. Commun.* **6**, 6556 (2015).
9. M. Huarte, The emerging role of lncRNAs in cancer. *Nat. Med.* **21**, 1253–1261 (2015).
10. M. Esteller, Non-coding RNAs in human disease. *Nat. Rev. Genet.* **12**, 861–874 (2011).
11. L. Statello, C.-J. Guo, L.-L. Chen, M. Huarte, Gene regulation by long non-coding RNAs and its biological functions. *Nat. Rev. Mol.* **22**, 96–118 (2021).

12. M. K. Iyer *et al.*, The landscape of long noncoding RNAs in the human transcriptome. *Nat. Genet.* **47**, 199–208 (2015).
13. M. Guttman, J. L. Rinn, Modular regulatory principles of large non-coding RNAs. *Nature* **482**, 339–346 (2012).
14. F. J. Slack, A. M. Chinnaiyan, The role of non-coding RNAs in oncology. *Cell* **179**, 1033–1055 (2019).
15. A. M. Schmitt, H. Y. Chang, Long noncoding RNAs in cancer pathways. *Cancer Cell* **29**, 452–463 (2016).
16. G. Arun, D. Aggarwal, D. L. Spector, MALAT1 long non-coding RNA: Functional implications. *Noncoding RNA* **6**, 22 (2020).
17. Y. Zhan *et al.*, Expression signatures of exosomal long non-coding RNAs in urine serve as novel non-invasive biomarkers for diagnosis and recurrence prediction of bladder cancer. *Mol. Cancer* **17**, 142 (2018).
18. G. Arun *et al.*, Differentiation of mammary tumors and reduction in metastasis upon MALAT1 lncRNA loss. *Genes Dev.* **30**, 34–51 (2016).
19. T. Gutschner *et al.*, The noncoding RNA MALAT1 is a critical regulator of the metastasis phenotype of lung cancer cells. *Cancer Res.* **73**, 1180–1189 (2013).
20. R. Sun *et al.*, Down-regulation of MALAT1 inhibits cervical cancer cell invasion and metastasis by inhibition of epithelial–mesenchymal transition. *Mol. Biosyst.* **12**, 952–962 (2016).
21. Z. H. Kwok, V. Roche, X. H. Chew, A. Fadieieva, Y. Tay, A non-canonical tumor suppressive role for the long non-coding RNA MALAT1 in colon and breast cancers. *Int. J. Cancer* **143**, 668–678 (2018).
22. Y. Han *et al.*, Tumor-suppressive function of long noncoding RNA MALAT1 in glioma cells by downregulation of MMP2 and inactivation of ERK/MAPK signaling. *Cell Death Dis.* **7**, e2123 (2016).
23. J. Kim *et al.*, Long noncoding RNA MALAT1 suppresses breast cancer metastasis. *Nat. Genet.* **50**, 1705–1715 (2018).
24. S. Xu *et al.*, Downregulation of long noncoding RNA MALAT1 induces epithelial-to-mesenchymal transition via the PI3K-AKT pathway in breast cancer. *Int. J. Clin. Exp. Pathol.* **8**, 4881–4891 (2015).
25. E. Tutucci *et al.*, An improved MS2 system for accurate reporting of the mRNA life cycle. *Nat. Methods* **15**, 81–89 (2018).
26. A. D. Cawte, P. J. Unrau, D. S. Rueda, Live cell imaging of single RNA molecules with fluorogenic Mango II arrays. *Nat. Commun.* **11**, 1283 (2020).
27. K. Kozyrska *et al.*, p53 directs leader cell behavior, migration, and clearance during epithelial repair. *Science* **375**, eabl8876 (2022).
28. G. Chrisafis *et al.*, Collective cancer cell invasion requires RNA accumulation at the invasive front. *Proc. Natl. Acad. Sci. U.S.A.* **117**, 27423–27434 (2020).
29. A. P. Young, D. J. Jackson, R. C. Wyeth, A technical review and guide to RNA fluorescence in situ hybridization. *PeerJ* **8**, e8806 (2020).
30. F. Ozsolak, P. M. Milos, RNA sequencing: Advances, challenges and opportunities. *Nat. Rev. Genet.* **12**, 87–98 (2011).
31. P. J. Santangelo, B. Nix, A. Tsourkas, G. Bao, Dual FRET molecular beacons for mRNA detection in living cells. *Nucleic Acids Res.* **32**, e57 (2004).
32. Y. Wan, N. Zhu, Y. Lu, P. K. Wong, DNA transformer for visualizing endogenous RNA dynamics in live cells. *Anal. Chem.* **91**, 2626–2633 (2019).
33. R. Riahi *et al.*, Detection of mRNA in living cells by double-stranded locked nucleic acid probes. *Analyst* **138**, 4777–4785 (2013).
34. S. A. Vilchez Mercedes, I. Eder, M. Ahmed, N. Zhu, P. K. Wong, Optimizing locked nucleic acid modification in double-stranded biosensors for live single cell analysis. *Analyst* **147**, 722–733 (2022).
35. J. Xu, S. Lamouille, R. Derynck, TGF-β-induced epithelial to mesenchymal transition. *Cell Res.* **19**, 156–172 (2009).
36. R. Riahi, Y. Yang, D. D. Zhang, P. K. Wong, Advances in wound-healing assays for probing collective cell migration. *J. Lab. Autom.* **17**, 59–65 (2012).
37. F. Bocci *et al.*, NRF2 activates a partial epithelial-mesenchymal transition and is maximally present in a hybrid epithelial/mesenchymal phenotype. *Integr. Biol.* **11**, 251–263 (2019).
38. S. A. Vilchez Mercedes *et al.*, Nrf2 modulates the hybrid epithelial/mesenchymal phenotype and notch signaling during collective cancer migration. *Front. Mol. Biosci.* **9**, 807324 (2022).
39. B. L. LeSavage, R. A. Suhar, N. Broguiere, M. P. Lutolf, S. C. Heilshorn, Next-generation cancer organoids. *Nat. Mater.* **21**, 143–159 (2022).
40. Y. Yang *et al.*, Probing leader cells in endothelial collective migration by plasma lithography geometric confinement. *Sci. Rep.* **6**, 22707 (2016).
41. M. Chen, Z. Xia, C. Chen, W. Hu, Y. Yuan, LncRNA MALAT1 promotes epithelial-to-mesenchymal transition of esophageal cancer through Ezh2-Notch1 signaling pathway. *Anticancer Drugs* **29**, 767–773 (2018).
42. C. Zhao, X. Ling, Y. Xia, B. Yan, Q. Guan, The m6A methyltransferase METTL3 controls epithelial-mesenchymal transition, migration and invasion of breast cancer through the MALAT1/miR-26b/HMGA2 axis. *Cancer Cell Int.* **21**, 441 (2021).
43. Z. Sun *et al.*, YAP1-induced MALAT1 promotes epithelial–mesenchymal transition and angiogenesis by sponging miR-126-5p in colorectal cancer. *Oncogene* **38**, 2627–2644 (2019).
44. Y. Zhou *et al.*, Study on mechanism about long noncoding RNA MALAT1 affecting pancreatic cancer by regulating Hippo-YAP signaling. *J. Cell. Physiol.* **233**, 5805–5814 (2018).
45. M. Zuker, Mfold web server for nucleic acid folding and hybridization prediction. *Nucleic Acids Res.* **31**, 3406–3415 (2003).
46. K. Jaqaman *et al.*, Robust single-particle tracking in live-cell time-lapse sequences. *Nat. Methods* **5**, 695–702 (2008).
47. J.-Y. Tinevez *et al.*, TrackMate: An open and extensible platform for single-particle tracking. *Methods* **115**, 80–90 (2017).